frontiers in Materials

ORIGINAL RESEARCH
published: 01 November 2019
doi: 10.3389/fmats.2019.00271

The Synergetic Effect of Ni and Fe Bi-metal Single Atom Catalysts on Graphene for Highly Efficient Oxygen Evolution Reaction

Yingqi Xu[1], Weifeng Zhang[1], Yaguang Li[1], Pengfei Lu[2], Yi Wang[2,3] and Zhong-Shuai Wu[2]**

[1] Hebei Key Lab of Optic-Electronic Information and Materials, The College of Physics Science and Technology, Hebei University, Baoding, China, [2] Dalian National Laboratory for Clean Energy, Dalian Institute of Chemical Physics, Chinese Academy of Sciences, Dalian, China, [3] University of Chinese Academy of Sciences, Beijing, China

Oxygen evolution reaction (OER) is key for electrochemical water splitting. Catalysts minimized in single-atom level (SACs) anchored on two-dimensional substances are highly active for various electrocatalytic reactions, but so far represent the limited performance for OER. Herein we report a general strategy for the fabrication of bi-metal Ni and Fe SACs loaded on graphene to significantly boost the OER activity. Notably, this unique structure of single Ni and Fe atoms co-existed on graphene has a strong synergetic effect, which can substantially elevate the charge transfer of catalysts. As a result, the obtained bi-metal SACs with the appropriate ratio of 4 for single Ni and Fe atoms show a small overpotential of 247 mV at 10 mA·cm^{-2} of OER current density in KOH electrolyte, outperforming individual-metal Ni (329 mV) or Fe (384 mV) SACs. Furthermore, such catalyst exhibits excellent stability without significant decay with increasing time at high current of 20 mA·cm^{-2} continuously for 48 h. This work provides a new avenue for regulating the properties of transition metal SACs on graphene for water electrolysis.

Keywords: single atom catalyst, bi-metal, synergetic effect, graphene, oxygen evolution reaction

OPEN ACCESS

Edited by:
Zhenhai Xia,
University of North Texas,
United States

Reviewed by:
Shichun Mu,
Wuhan University of Technology, China
Jialiang Wang,
University of Wisconsin-Madison,
United States

Correspondence:
Yaguang Li
yaguang_1987@126.com
Zhong-Shuai Wu
wuzs@dicp.ac.cn

Specialty section:
This article was submitted to Energy Materials, a section of the journal Frontiers in Materials

Received: *30 August 2019*
Accepted: *16 October 2019*
Published: *01 November 2019*

Citation:
Xu Y, Zhang W, Li Y, Lu P, Wang Y and Wu Z-S (2019) The Synergetic Effect of Ni and Fe Bi-metal Single Atom Catalysts on Graphene for Highly Efficient Oxygen Evolution Reaction. Front. Mater. 6:271. doi: 10.3389/fmats.2019.00271

INTRODUCTION

Water splitting utilized by electric energy is an efficient way for the store of discontinuous and sustainable energies (Fan et al., 2016; Seitz et al., 2016; Zhang B. et al., 2016). Among the reactions in electrochemical water splitting, oxygen evolution reaction (OER) is a kinetically slow process, which is a big obstacle in electrochemical water splitting (Long et al., 2014; Zhang Y. et al., 2016; Suen et al., 2017). Therefore, rational design of highly active and durable OER catalysts is the key theme in water splitting (Gong et al., 2013; Ling et al., 2016; Zhuang et al., 2017). Single atom structure represents the lowest size limit on synthesizing catalysts (Qiao et al., 2011), which has been regarded as the frontier of catalysis (Liu et al., 2016). Among them, single atom catalysts (SACs) have shown great potential for hydrogen evolution reaction and oxygen reduction reaction (Fei et al., 2015; Qiu et al., 2015; Zhang L. et al., 2017). Although a sequence of OER sensitive metals (e.g. Ni, Co) have been synthesized in atoms form (Fei et al., 2015; Chen et al., 2017; Zhao et al., 2017), their OER activities are still unsatisfactory.

In our previous work (Xu et al., 2020), we have changed the coordination elements of single nickel atoms from nitrogen to oxygen to activate the OER activity. This restructured single nickel

atoms for OER shows a small overpotential of 330 mV level at current density of 10 mA·cm^{-2}, which is even equivalent to the benchmark OER catalysts of NiFe layer double hydroxide (LDH) (Han et al., 2016; Lu et al., 2017). However, with unremitting efforts on developing multiple metal compounds, the overpotential at 10 mA·cm^{-2} has reached up to 200 mV level (Qian et al., 2017; Yao et al., 2018; Zhang P. et al., 2018). SACs are still far from the best catalysts available for OER. At present, the best OER catalysts include metal oxides (Yin et al., 2010; Zhou et al., 2018), hydroxides (Balogun et al., 2016; Liu et al., 2017), perovskites (Zhang Y. et al., 2017), phosphides etc. (Zhao et al., 2016; Hu et al., 2017). It is worth noting that the composition combination of different metal elements could greatly improve the OER activity of catalysts. As a well-known example, the OER activity of Ni can be promoted by the synergistic effect of Fe in NiFe LDH, which outperforms those of the corresponding single-Ni or Fe oxides (Trotochaud et al., 2012; Gong et al., 2013). It is indicated that the interaction between heterogeneous elements can significantly change the catalytic activity of materials.

To improve the OER activity of SACs, we considered whether the synergetic effect of dual-metal SACs could be applied on OER. In this work, we focus on realizing the synergetic effect between different single atoms. We synthesized dual-metal SACs of Ni, Fe elements on graphene

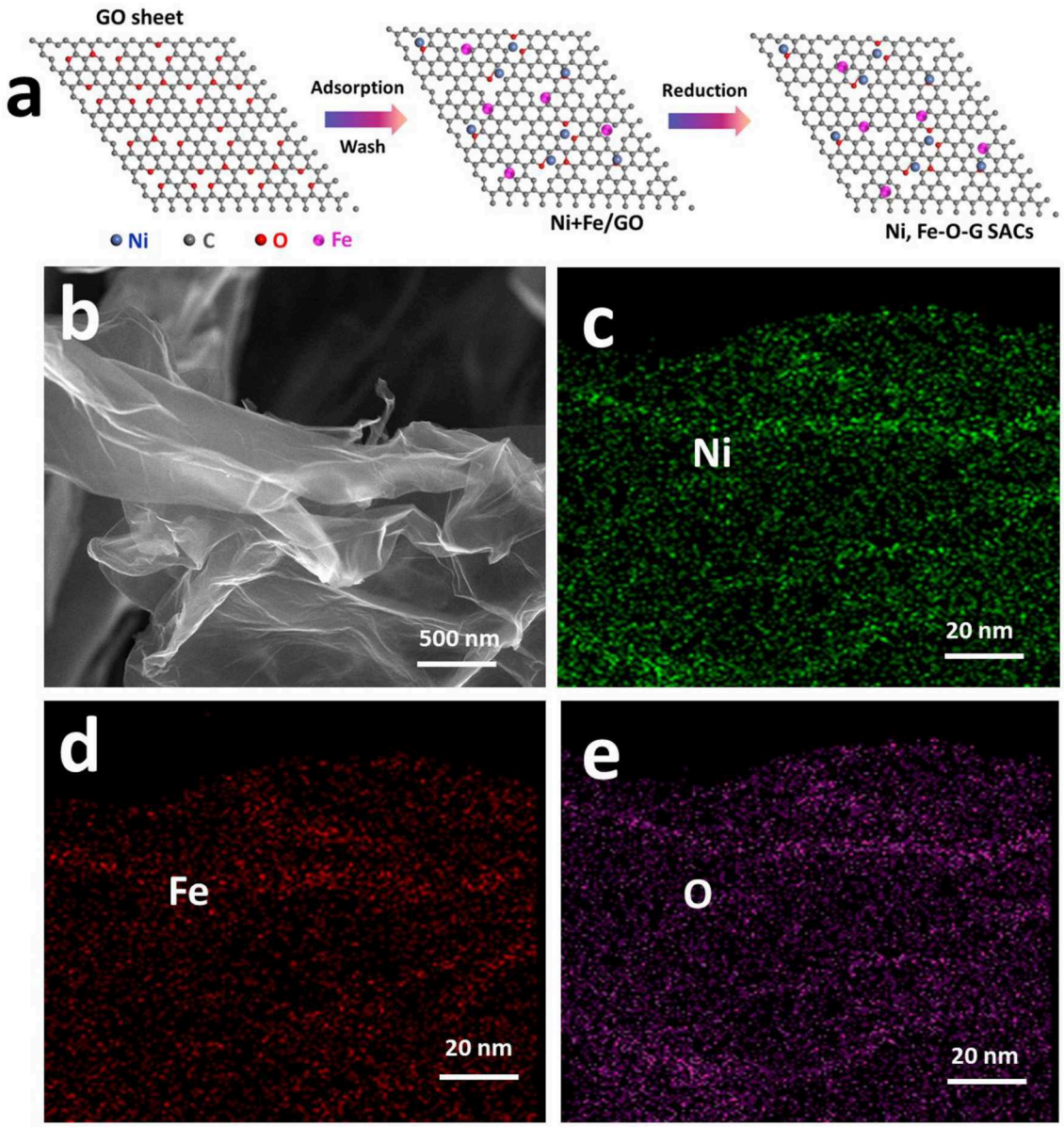

FIGURE 1 | (a) Schematic synthesis of Ni, Fe-O-G SACs. **(b)** SEM image of Ni_4Fe_1-O-G SACs. **(c–e)** elemental mapping images of Ni, Fe, O elements through the sheet of Ni_4Fe_1-O-G SACs.

simultaneously (denoted as Ni, Fe-O-G SACs) by ions adsorption and graphene oxide (GO) templated method. The coupling effect of Ni, Fe single atoms could efficiently boost the activity and charge transfer of Ni, Fe-O-G SACs by tuning the Ni/Fe ratio. Impressively, Ni, Fe-O-G SACs for OER achieved a low overpotential of 247 mV at current density of 10 $mA \cdot cm^{-2}$ when the ratio of Ni and Fe was 4. It was significantly lower than those of solely single Ni atoms on graphene (329 mV) and solely single Fe atoms on graphene (384 mV).

EXPERIMENTAL SECTION

Preparation of Ni, Fe-O-G SACs

Firstly, 100 mL GO aqueous solution (2 mg/mL) was stirred for 0.5 h with a controllable amount of $Ni(NO_3)_2 \cdot 6H_2O$ and $Fe(NO_3)_3 \cdot 9H_2O$. After washing three times with assistance of centrifugation, the metal ions not adsorbed on GO were fully removed. Then, the obtained sample was further dispersed in 30 mL deionized water, and freeze-dried within 2 days to remove residual water. Afterwards, the dried sample was heated at 95°C for 24 in hydrazine vapor to form Ni, Fe-O-G SACs. Note that the Ni/Fe ratio in Ni, Fe-O-G SACs was easily controlled by changing the amount of Ni^{2+} and Fe^{3+} salts and the details was listed in **Table S1**.

Characterizations

The X-ray diffraction (XRD, BRUKER, D8 ADVANCE), scanning electron microscopy (SEM, FEI Nova Nano SEM450), transmission electron microscopy (TEM, JEOL 2100F) and scanning transmission electron microscopy (STEM, JEOL, ARM-200F) are used to characterize the morphology, crystal structure and atomic dispersion of samples. The X-ray photoelectron spectroscopic (XPS) spectra were detected by Thermo ESCALAB-250 spectrometer with a monochromatic Al Kα radiation source (1486.6 eV). The binding energies determined by XPS were corrected with reference of adventitious carbon peak (284.6 eV) for each sample. The X-ray absorption near-edge structure (XANES) and extended X-ray absorption fine structure (EXAFS) spectra at Ni, Fe K-edges were collected by the beamline of BL14W1 at Shanghai Synchrotron Radiation facility (SSRF). Then, we used Athena software to analyze those spectra.

Electrochemical Measurements

To measure the electrode for OER test, firstly, carbon cloth cut into the square (1 cm^2) was soaked by ethanol and water. Secondly, 10 mg catalyst was added into 2.0 mL of ethanol and 0.01 mL of Nafion solution (5.0 wt%). Thirdly, the catalyst was dispersed by sonication to form an ink. Finally, 0.1 mL ink was dropped into the washed carbon cloth and dried for 0.5 h in air. The loading amount of catalysts was 0.5 mg cm^{-2}.

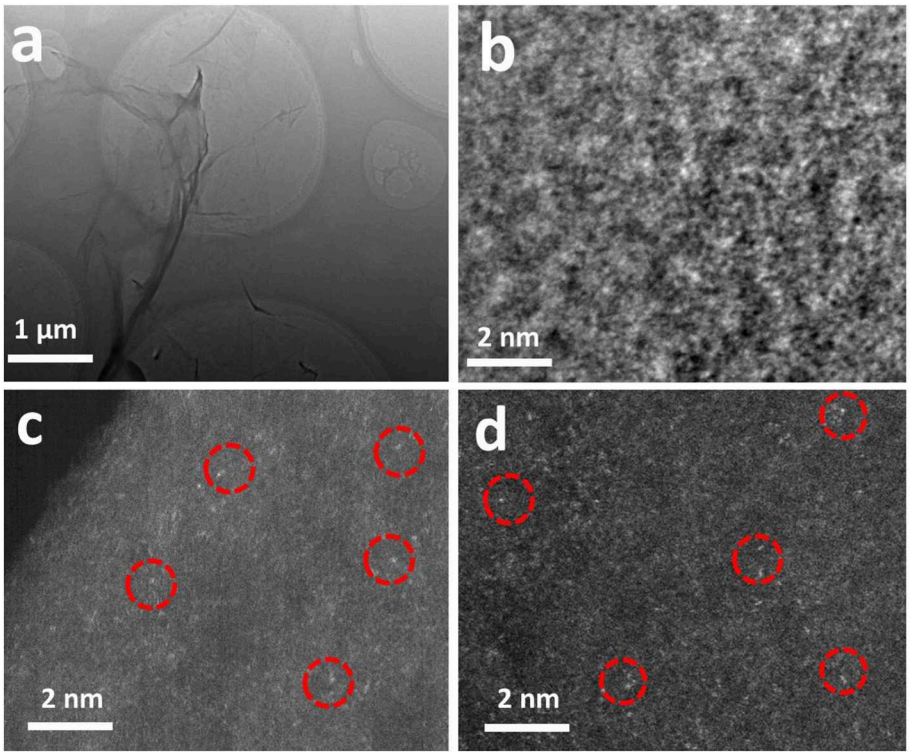

FIGURE 2 | (a) TEM image of Ni_4Fe_1-O-G SACs. **(b)** HRTEM image of Ni_4Fe_1-O-G SACs. **(c,d)** Magnified HAADF-STEM images of Ni_4Fe_1-O-G SACs. The single Ni, Fe atoms were marked with red circles.

The electrochemical workstation (Zennium_Pro, Zahner, Germany) was used to detect the OER performances of those catalysts with the counter electrode of Pt square sheet (4 cm^2) and a reference electrode of Ag/AgCl. The potentials were calibrated by the reversible hydrogen electrode (RHE), by the following equation:

$$E_{\mathrm{RHE}}\,(\mathrm{V}) = E_{\mathrm{Ag/AgCl}} + 0.197\,\mathrm{V} + 0.059\times \mathrm{pH}$$
$$\text{Overpotential} = E_{\mathrm{RHE}} - 1.23\,(\mathrm{V}).$$

Before OER tests, the electrodes attached with catalysts were pre-scanned by cyclic voltammetric to stable the OER activity. The scan rate of linear scan voltammetry (LSV) was 2 mV s^{-1}. The *iR*-correction was 80%. Electrochemical impedance spectroscopy (EIS) was tested by potentiostatic mode at 1.26 V vs. RHE with scanning frequency from 1.0 MHz to 0.05 Hz.

RESULTS AND DISCUSSIONS

As shown in **Figure 1a**, to synthesize the graphene (G) sheets decorated with single atoms of Ni and Fe, firstly, moderate amount of Ni^{2+} and Fe^{3+} salts were dissolved in GO aqueous solution. Since GO are rich in hydroxyl and carboxyl groups, Ni^{2+} and Fe^{3+} ions were readily adsorbed on the surface of GO sheets via the functional oxygenated groups, e.g., hydroxyls and carboxyls (Gao et al., 2017). Secondly, the Ni^{2+} and Fe^{3+} ions not adsorbed on GO sheets were removed by washing process, and the washed GO solution were frozen within 2 days. Finally, hydrazine vapor was used for the reduction of GO into graphene at 95°C for 24 h to obtain Ni, Fe-O-G SACs (Sun et al., 2013). The Ni/Fe ratio on graphene could be readily controlled by changing the amount of Ni^{2+} and Fe^{3+} salts (**Table S1**). XRD pattern of the as-obtained Ni, Fe-O-G SACs with Ni/Fe ratio of 4 (abbreviated as Ni_4Fe_1-O-G SACs) presented two broad diffraction peaks at 23.2° and 43.6°, derived from the graphene. Besides this, no peaks of Ni metals, metal oxides and carbides were observed (**Figure S1a**) (Liu et al., 2018). Raman spectrum confirmed the existence of oxygen and defects on graphene in this sample (Iwase et al., 2011), indicative of the incorporation of oxygen into graphene (**Figure S1b**). SEM image showed the soft nanosheets morphology of Ni_4Fe_1-O-G SACs (**Figure 1b**). Elemental mapping images revealed the even dispersion of Ni, Fe and O elements on the sheets of Ni_4Fe_1-O-G SACs (**Figures 1c–e**). TEM image revealed the absence of aggregates on the nanosheet of Ni_4Fe_1-O-G SACs (**Figure 2a**), which was in line with the HRTEM result, depicting no lattice fringes (**Figure 2b**). Aberration-corrected STEM (**Figures 2c,d**) was allowed for the direct observation of atomic dispersion of Fe and Ni. In the STEM images of Ni_4Fe_1-O-G SACs, the metal atoms appeared as light points were individually located on graphene (marked by red circles). There was no sub-nanometer clusters presented. Considering that C and O elements had a

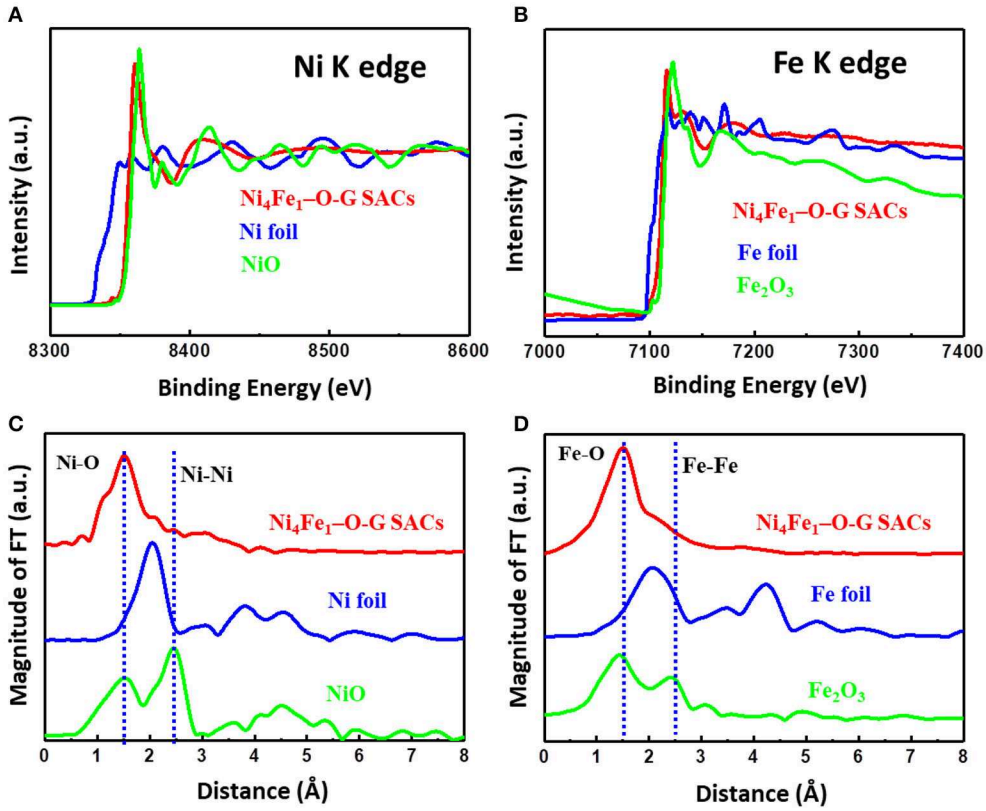

FIGURE 3 | (A) Ni K-edge XANES of Ni_4Fe_1-O-G SACs, Ni foil and NiO. **(B)** Fe K-edge XANES of Ni_4Fe_1-O-G SACs, Fe foil and Fe_2O_3. **(C)** Ni K-edge FT-EXAFS spectra of Ni_4Fe_1-O-G SACs with references of Ni foil and NiO. **(D)** Fe K-edge FT-EXAFS spectra of Ni_4Fe_1-O-G SACs with references of Fe foil and Fe_2O_3.

smaller atomic number than Fe and Ni, the atomic level spots should be Fe and Ni atoms, manifesting as single atoms away from each other. Thus, Ni and Fe were uniformly dispersed on the surface of graphene in single atomic form. The Ni and Fe 2p XPS spectra of Ni_4Fe_1-O-G SACs were presented in **Figure S2**. The Ni $2p_{3/2}$, $2p_{1/2}$ and Fe $2p_{3/2}$, $2p_{1/2}$ peaks of Ni_4Fe_1-O-G SACs were obtained at 873.9 eV, 856.3 eV and 724.1 eV, 712.2 eV respectively, assigned to the Ni (II) and Fe(III) species (Zhang Y. et al., 2011; Yan et al., 2012).

Further, the spectra of XANES and EXAFS were used to verify the possible bonding forms between nickel, iron and the light elements in Ni_4Fe_1-O-G SACs, in comparison with NiO, Fe_2O_3 and Ni, Fe foil. As seen from the curves of XANES (**Figures 3A,B**), the E_0 values of Ni, Fe K-edges followed the order of Ni_4Fe_1-O-G SACs = NiO, Fe_2O_3 > Ni, Fe foils. Since higher E_0 corresponds to higher oxidation state, it is suggested that the valence states of Fe and Ni species in Ni_4Fe_1-O-G SACs are +2 and +3, respectively, identical to the XPS results. Further, the coordination environment of Ni and Fe in Ni_4Fe_1-O-G SACs was elucidated by the Fourier-transformed EXAFS (FT-EXAFS, **Figures 3C,D**), in which showed only notable peaks of Ni-O, Fe-O coordination, similar to the peaks of NiO, Fe_2O_3 at ∼1.6 Å (Yan et al., 2018). Moreover, no appearance of Ni-Ni and Fe-Fe coordination peaks at 2.6 Å were detected. Consequently, FT-EXAFS results evidenced the atomic level dispersion of Ni-O-graphene and Fe-O-graphene structures in Ni_4Fe_1-O-G SACs.

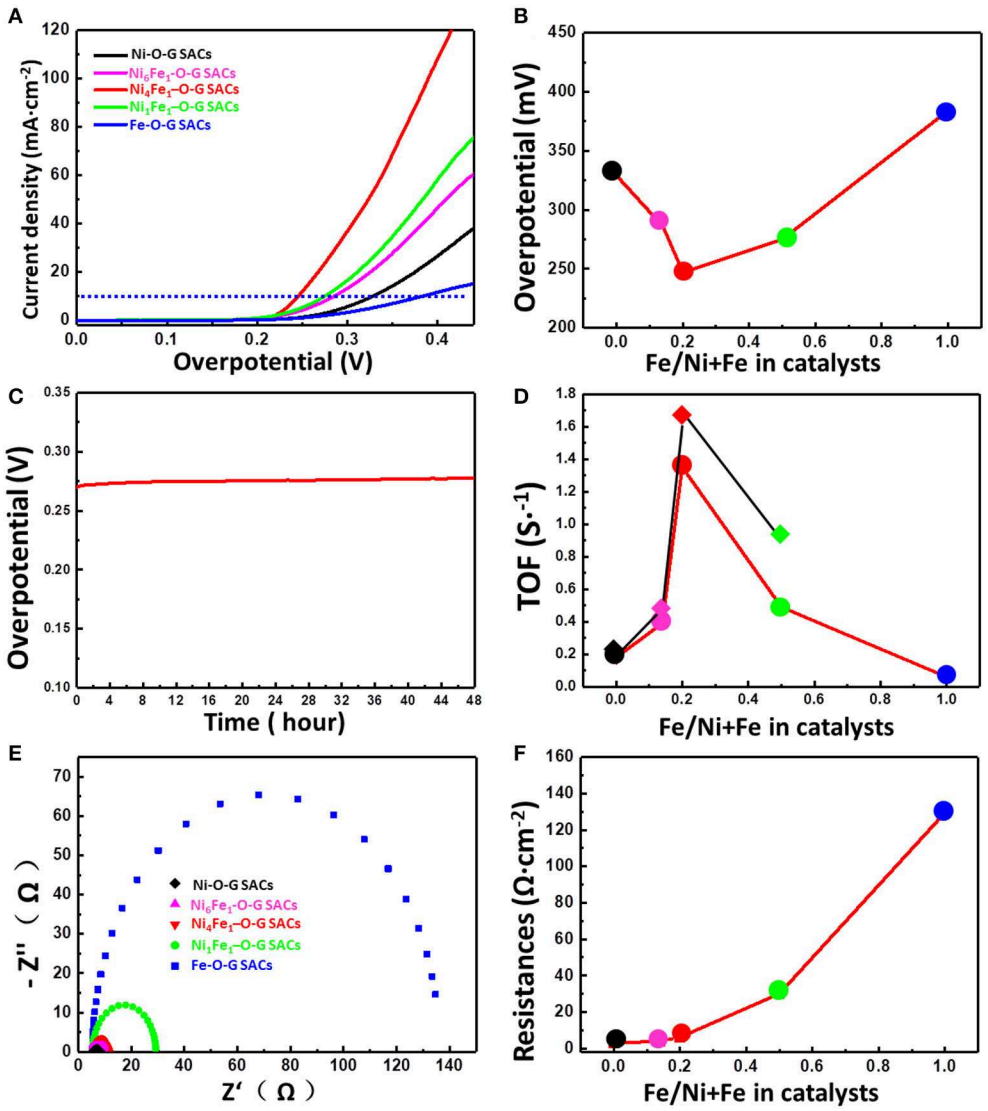

FIGURE 4 | (A) The OER polarization curves of Ni, Fe-O-G SACs with different Ni, Fe ratio (Ni, Ni_6Fe_1, Ni_4Fe_1, Ni_1Fe_1, Fe) obtained at scan rate of 2 mV s^{-1} and 80% *iR* correction. **(B)** The corresponding required overpotential of Ni, Fe-O-G SACs for 10 mA cm^{-2} current density. **(C)** Chronopotentiometric curve of Ni_4Fe_1-O-G SACs maintained at 20 mA cm^{-2} current density, in 1 M KOH, with 80% *iR* correction. **(D)** The TOF value at 300 mV overpotential of Ni, Fe-O-G SACs with different Ni, Fe ratio (Ni, Ni_6Fe_1, Ni_4Fe_1, Ni_1Fe_1, Fe), obtained at scan rate of 2 mV s^{-1} and 80% *iR* correction. **(E)** Nyquist plots of Ni, Fe-O-G SACs with different Ni, Fe ratio (Ni, Ni_6Fe_1, Ni_4Fe_1, Ni_1Fe_1, Fe). **(F)** The corresponding charge resistances.

To show the excellent catalytic activity of Ni, Fe-O-G SACs and highlight the activity of Ni, Fe-O-G SACs affected by the coupling effect of Ni and Fe, we also synthesized the Ni, Fe-O-G SACs with different Ni and Fe ratios, ranging from 0, 0.14, 0.2, 0.5, to 1 of Fe/Ni+Fe ratio (**Figures S3, S4**; **Table S2**). Remarkably, the Ni_4 Fe_1-O-G SACs possessed the best OER activity among these samples (**Figure 4A**; **Figure S5**). To generate a current density of 10 mA·cm^{-2}, Ni_4Fe_1-O-G SACs only need an overpotential of 247 mV, which was much smaller than those of Ni-O-G SACs (329 mV) and Fe-O-G SACs (384 mV) (**Figure 4B**), and the Ni based reported OER catalysts, e.g., NiO film (540 mV) (Nardi et al., 2015), Ni/N doped graphene (397 mV) (Chen et al., 2013), Ni_2P/NiO_x (286 mV) (Stern et al., 2015), $Ni_{11}(HPO_3)_8(OH)_6$ (274 mV) (Menezes et al., 2018), Ni_3Se_2 (290 mV), Ni SAC/defected graphene (270 mV) (Zhang L. et al., 2018).

To demonstrate the long-term stability of Ni_4Fe_1-O-G SACs, continuous water oxidation at a current density of 20 mA·cm^{-2} was examined for 48 h (**Figure 4C**). Obviously, the overpotential showed little change with increasing time, showing excellent durability of Ni_4Fe_1-O-G SACs for OER. Further, **Figure 4B** showed that the overpotential of Ni_4Fe_1-O-G SACs was also lower than those of Ni_6Fe_1-O-G SACs (286 mV) and Ni_1Fe_1-O-G SACs (275 mV), when the OER current density was 10 mA·cm^{-2}. It is revealed that the ratio of Ni/Fe in Ni, Fe-O-G SACs has a great influence on the OER activity of the catalysts. Since the number of Ni+Fe atoms was not equal on different Ni, Fe-O-G SACs, the simple comparison of OER currents did not objectively reflect with the activity of single atoms. Therefore, we used the turnover frequencies (TOFs) of oxygen production at overpotential of 300 mV (with 80% *iR* correction) to quantify the intrinsic activity of Ni and Fe single atoms in different Ni, Fe-O-G SACs. It is assumed that all the Ni and Fe atoms in Ni, Fe-O-G SACs were totally taking part in OER. The TOF values calculated from Ni-O-G SACs, Ni_6Fe_1-O-G SACs, Ni_4Fe_1-O-G SACs, Ni_1Fe_1-O-G SACs and Fe-O-G SACs were 0.18, 0.39, 1.35, 0.49, and 0.06 s^{-1}, respectively (**Figure 4D**), confirming that the single atoms in Ni_4Fe_1-O-G SACs own the highest OER activity among all the Ni, Fe-O-G SACs. On the other hand, it has been reported that the Fe atoms are not very active for OER (Li et al., 2017). Therefore, we further calculated the TOF of those catalysts assuming only Ni atoms active for OER. In this case, the TOF values calculated from Ni-O-G SACs, Ni_6Fe_1-O-G SACs, Ni_4Fe_1-O-G SACs and Ni_1Fe_1-O-G SACs were 0.18, 0.45, 1.68, and 0.98 s^{-1}, respectively (**Figure 4D**), which further confirmed the higher OER activity of Ni_4Fe_1-O-G SACs mainly from Ni atoms. Previously, Nocera et al. have reported that the Fe^{3+} could promote the formation of high valence Ni atoms during OER process, which possibly generated more active Ni sites to acquire better OER activity through the introduction of the increased amount of Fe^{3+} (Li et al., 2017). However, our experimental results showed that the OER activity was not linearly improved by increasing the Fe ratio in Ni, Fe-O-G SACs, indicating that other factors also affected the OER activity. We then tested the electrical conductivity of Ni, Fe-O-G SACs, derived from electrochemical impedance spectroscopy (EIS). As shown in **Figure 4E**, the semicircle curves of EIS were expanded with increasing Fe ratio in Ni, Fe-O-G SACs. **Figure 4F** showed that the charge transfer resistance (*R*) of Ni-O-G SACs, Ni_6Fe_1-O-G SACs, Ni_4Fe_1-O-G SACs, and Ni_1Fe_1-O-G SACs, Fe-O-G SACs was 2.9, 4.0, 6.2, 30.1, and 129.4 Ω·cm^{-2}, respectively. This result suggested the higher iron ratio in Ni, Fe-O-G SACs increased the *R* to block the charge transfer between active sites and electrode, thus limiting the OER current density.

In summary, we reported a versatile strategy of 2D GO template-based bi-metal ion adsorption to create Ni, Fe-O-G SACs with strong coupled nickel-oxygen and iron-oxygen bonding as highly active and durable OER electrocatalysts. The multiple characterizations revealed that the bi-metals of Ni and Fe elements were individually anchored on the oxygen-containing sites of graphene in single atomic form. Through the full optimization of the Fe, Ni ratio, it was demonstrated that Ni_4Fe_1-O-G SACs for OER showed the low overpotential of only 247 mV at current density of 10 mA·cm^{-2}, 48 h long-life durability without significant degradation, 1.35 s^{-1} of oxygen production TOF at overpotential of 300 mV. Therefore, this strong coupling effect of bi-metal SACs on graphene and other 2D materials will open many intriguing opportunities for designing complex SACs as efficient and robust OER catalysts.

DATA AVAILABILITY STATEMENT

The datasets generated for this study are available on request to the corresponding author.

AUTHOR CONTRIBUTIONS

YL and Z-SW conceived this project. YX, WZ, PL, and YW performed the catalyst preparation and characterizations. YX, YL, and Z-SW analyzed the data and wrote the manuscript. All the authors discussed the results and commented on the manuscript.

FUNDING

This work was supported by the National Key R&D Program of China (Grants 2016YFB0100100, and 2016YFA0200200), National Nature Science Foundation of China (Grants 51702078, 51872283 and 51572259), Liao Ning Revitalization Talents Program (Grant XLYC1807153), Natural Science Foundation of Liaoning Province (Grant 20180510038), DICP (DICP ZZBS201708, DICP ZZBS201802), DICP&QIBEBT (Grant DICP&QIBEBT UN201702), Dalian National Laboratory For Clean Energy (DNL), CAS, and DNL Cooperation Fund, CAS (DNL180310, DNL180308). We thank SSRF for the beamline (BL14W1) and assistance with the EXAFS test. Thanks for the TEM technical supports provided by the Microanalysis Center, College of Physics Science and Technology, Hebei University.

SUPPLEMENTARY MATERIAL

The Supplementary Material for this article can be found online at: https://www.frontiersin.org/articles/10.3389/fmats.2019.00271/full#supplementary-material

REFERENCES

Balogun, M.-S., Qiu, W., Yang, H., Fan, W., Huang, Y., Fang, P., et al. (2016). A monolithic metal-free electrocatalyst for oxygen evolution reaction and overall water splitting. *Energy Environ. Sci.* 9, 3411–3416. doi: 10.1039/C6EE01930G

Chen, S., Duan, J., Ran, J., Jaroniec, M., and Qiao, S. Z. (2013). N-doped graphene film-confined nickel nanoparticles as a highly efficient three-dimensional oxygen evolution electrocatalyst. *Energy Environ. Sci.* 6, 3693–3699. doi: 10.1039/c3ee42383b

Chen, Y., Ji, S., Wang, Y., Dong, J., Chen, W., Li, Z., et al. (2017). Isolated single iron atoms anchored on N-doped porous carbon as an efficient electrocatalyst for the oxygen reduction reaction. *Angew. Chem. Int. Ed.* 56, 6937–6941. doi: 10.1002/anie.201702473

Fan, L., Liu, P. F., Yan, X., Gu, L., Yang, Z. Z., Yang, H. G., et al. (2016). Atomically isolated nickel species anchored on graphitized carbon for efficient hydrogen evolution electrocatalysis. *Nat. Commun.* 7:10667. doi: 10.1038/ncomms10667

Fei, H., Dong, J., Arellano-Jiménez, M. J., Ye, G., Dong Kim, N., Samuel, E. L., et al. (2015). Atomic cobalt on nitrogen-doped graphene for hydrogen generation. *Nat. Commun.* 6:8668. doi: 10.1038/ncomms9668

Gao, L., Li, Y., Xiao, M., Wang, S., Fu, G., and Wang, L. (2017). Synthesizing new types of ultrathin 2D metal oxide nanosheets via half-successive ion layer adsorption and reaction. *2D Mater.* 4:025031. doi: 10.1088/2053-1583/aa5b1b

Gong, M., Li, Y., Wang, H., Liang, Y., Wu, J. Z., Zhou, J., et al. (2013). An advanced Ni-Fe layered double hydroxide electrocatalyst for water oxidation. *J. Am. Chem. Soc.* 135, 8452–8455. doi: 10.1021/ja4027715

Han, L., Dong, S., and Wang, E. (2016). Transition-metal (Co, Ni, and Fe)-based electrocatalysts for the water oxidation reaction. *Adv. Mater.* 28, 9266–9291. doi: 10.1002/adma.201602270

Hu, F., Zhu, S., Chen, S., Li, Y., Ma, L., Wu, T., et al. (2017). Amorphous metallic NiFeP: a conductive bulk material achieving high activity for oxygen evolution reaction in both alkaline and acidic media. *Adv. Mater.* 29:1606570. doi: 10.1002/adma.201606570

Iwase, A., Ng, Y. H., Ishiguro, Y., Kudo, A., and Amal, R. (2011). Reduced graphene oxide as a solid-state electron mediator in Z-scheme photocatalytic water splitting under visible light. *J. Am. Chem. Soc.* 133, 11054–11057. doi: 10.1021/ja203296z

Li, N., Bediako, D. K., Hadt, R. G., Hayes, D., Kempa, T. J., von Cube, F., et al. (2017). Influence of iron doping on tetravalent nickel content in catalytic oxygen evolving films. *Pro. Natl. Acad. Sci. U.S.A.* 114, 1486–1491. doi: 10.1073/pnas.1620787114

Ling, T., Yan, D. Y., Jiao, Y., Wang, H., Zheng, Y., Zheng, X., et al. (2016). Engineering surface atomic structure of single-crystal cobalt (II) oxide nanorods for superior electrocatalysis. *Nat. Commoun.* 7:12876. doi: 10.1038/ncomms12876

Liu, P., Zhao, Y., Qin, R., Mo, S., Chen, G., Gu, L., et al. (2016). Photochemical route for synthesizing atomically dispersed palladium catalysts. *Science* 352, 797–800. doi: 10.1126/science.aaf5251

Liu, W., Chen, Y., Qi, H., Zhang, L., Yan, W., Liu, X., et al. (2018). A durable nickel single-atom catalyst for hydrogenation reactions and cellulose valorization under harsh conditions. *Angew. Chem. Int. Ed.* 57, 7071–7075. doi: 10.1002/anie.201802231

Liu, Z., Zhao, Z., Wang, Y., Dou, S., Yan, D., Liu, D., et al. (2017). *In situ* exfoliated, edge-rich, oxygen-functionalized graphene from carbon fibers for oxygen electrocatalysis. *Adv. Mater.* 29:1606207. doi: 10.1002/adma.201606207

Long, X., Li, J., Xiao, S., Yan, K., Wang, Z., Chen, H., et al. (2014). A strongly coupled graphene and FeNi double hydroxide hybrid as an excellent electrocatalyst for the oxygen evolution reaction. *Angew. Chem. Int. Ed.* 53, 7584–7588. doi: 10.1002/anie.201402822

Lu, Z., Wang, J., Shifei, H., and Hou, Y. (2017). N,B-codoped defect-rich graphitic carbon nanocages as high performance multifunctional electrocatalysts. *Nano Energy.* 42, 334–340. doi: 10.1016/j.nanoen.2017.11.004

Menezes, P. W., Panda, C., Loos, S., Bunschei-Bruns, F., Walter, C., Schwarze, M., et al. (2018). A structurally versatile nickel phosphite acting as a robust bifunctional electrocatalyst for overall water splitting. *Energy Environ. Sci.* 11, 1287–1298. doi: 10.1039/C7EE03619A

Nardi, K. L., Yang, N., Dickens, C. F., Strickler, A. L., and Bent, S. F. (2015). Creating highly active atomic layer deposited NiO electrocatalysts for the oxygen evolution reaction. *Adv. Energy Mater.* 5:1500412. doi: 10.1002/aenm.201500412

Qian, M., Cui, S., Jiang, D., Zhang, L., and Du, P. (2017). Highly efficient and stable water-oxidation electrocatalysis with a very low overpotential using FeNiP substitutional-solid-solution nanoplate arrays. *Adv. Mater.* 29:1704075. doi: 10.1002/adma.201704075

Qiao, B., Wang, A., Yang, X., Allard, L. F., Jiang, Z., Cui, Y., et al. (2011). Single-atom catalysis of CO oxidation using Pt_1/FeO_x. *Nat. Chem.* 3, 634–641. doi: 10.1038/nchem.1095

Qiu, H. J., Ito, Y., Cong, W., Tan, Y., Liu, P., Hirata, A., et al. (2015). Nanoporous graphene with single-atom nickel dopants: an efficient and stable catalyst for electrochemical hydrogen production. *Angew. Chem. Int. Ed.* 54, 14031–14035. doi: 10.1002/anie.201507381

Seitz, L. C., Dickens, C. F., Nishio, K., Hikita, Y., Montoya, J., Doyle, A., et al. (2016). A highly active and stable $IrO_x/SrIrO_3$ catalyst for the oxygen evolution reaction. *Science* 353, 1011–1014. doi: 10.1126/science.aaf5050

Stern, L.-A., Feng, L., Song, F., and Hu, X. (2015). Ni_2P as a Janus catalyst for water splitting: the oxygen evolution activity of Ni_2P nanoparticles. *Energy Environ. Sci.* 8, 2347–2351. doi: 10.1039/C5EE01155H

Suen, N. T., Hung, S. F., Quan, Q., Zhang, N., Xu, Y. J., and Chen, H. M. (2017). Electrocatalysis for the oxygen evolution reaction: recent development and future perspectives. *Chem. Soc. Rev.* 46, 337–365. doi: 10.1039/C6CS00328A

Sun, H., Xu, Z., and Gao, C. (2013). Multifunctional, ultra-flyweight, synergistically assembled carbon aerogels. *Adv. Mater.* 25, 2554–2560. doi: 10.1002/adma.201204576

Trotochaud, L., Ranney, J. K., Williams, K. N., Boettcher, S. W., Trotochaud, L., Ranney, J. K., et al. (2012). Solution-cast metal oxide thin film electrocatalysts for oxygen evolution. *J. Am. Chem. Soc.* 134, 17253–17261. doi: 10.1021/ja307507a

Xu, Y., Zhang, W., Li, Y., Lu, P., and Wu, Z.-S. (2020). A general bimetal-ion adsorption strategy to prepare nickel single atom catalysts anchored on graphene for efficient oxygen evolution reaction. *J. Energy Chem.* 43, 52–57. doi: 10.1016/j.jechem.2019.08.006

Yan, C., Li, H., Ye, Y., Wu, H., Cai, F., Si, R., et al. (2018). Coordinatively unsaturated nickel-nitrogen sites towards selective and high-rate CO_2 electroreduction. *Energy Environ. Sci.* 11, 1204–1210. doi: 10.1039/C8EE00133B

Yan, J., Fan, Z., Sun, W., Ning, G., Wei, T., Zhang, Q., et al. (2012). Advanced asymmetric supercapacitors based on $Ni(OH)_2$/graphene and porous graphene electrodes with high energy density. *Adv. Funct. Mater.* 22, 2632–2641. doi: 10.1002/adfm.201102839

Yao, Y., Xu, Z., Cheng, F., Li, W., Cui, P., Xu, G., et al. (2018). Unlocking the potential of graphene for water oxidation using an orbital hybridization strategy. *Energy Environ. Sci.* 11, 407–416. doi: 10.1039/C7EE02972A

Yin, Q., Tan, J. M., Besson, C., Geletii, Y. V., Musaev, D. G., Kuznetsov, A. E., et al. (2010). A fast soluble carbon-free molecular water oxidation catalyst based on abundant metals. *Science* 328, 342–345. doi: 10.1126/science.1185372

Zhang, B., Zheng, X., Voznyy, O., Comin, R., Bajdich, M., García-Melchor, M., et al. (2016). Homogeneously dispersed multimetal oxygen-evolving catalysts. *Science* 352, 333–337. doi: 10.1126/science.aaf1525

Zhang, L., Han, L., Liu, H., Liu, X., and Luo, J. (2017). Potential-cycling synthesis of single platinum atoms for efficient hydrogen evolution in neutral media. *Angew. Chem. Int. Ed.* 56, 13694–13698. doi: 10.1002/anie.201706921

Zhang, L., Jia, Y., Gao, G., Yan, X., Chen, N., Chen, J., et al. (2018). Graphene defects trap atomic Ni species for hydrogen and oxygen evolution reactions. *Chem.* 4, 285–297. doi: 10.1016/j.chempr.2017.12.005

Zhang, P., Li, L., Nordlund, D., Chen, H., Fan, L., Zhang, B., et al. (2018). Dendritic core-shell nickel-iron-copper metal/metal oxide electrode for efficient electrocatalytic water oxidation. *Nat. Commun.* 9:381. doi: 10.1038/s41467-017-02429-9

Zhang, Y., Fan, X., Jian, J., Yu, D., Zhang, Z., and Dai, L. (2017). A general polymer-assisted strategy enables unexpected efficient metal-free oxygen-evolution catalysis on pure carbon nanotubes. *Energy Environ. Sci.* 10, 2312–2317. doi: 10.1039/C7EE01702B

Zhang, Y., Ouyang, B., Xu, J., Jia, G., Chen, S., Rawat, R. S., et al. (2016). Rapid synthesis of cobalt nitride nanowires: highly efficient and low-cost

catalysts for oxygen evolution. *Angew. Chem. Int. Ed.* 55, 8670–8674. doi: 10.1002/anie.201604372

Zhang, Y., Xu, F., Sun, Y., Shi, Y., Wenab, Z., and Li, Z., et al. (2011). Assembly of $Ni(OH)_2$ nanoplates on reduced graphene oxide: a two dimensional nanocomposite for enzyme-free glucose sensing. *J. Mater. Chem.* 21, 16949–16954. doi: 10.1039/c1jm11641j

Zhao, C., Dai, X., Yao, T., Chen, W., Wang, X., Wang, J., et al. (2017). Ionic exchange of metal-organic frameworks to access single nickel sites for efficient electroreduction of CO_2. *J. Am. Chem. Soc.* 139, 8078–8081. doi: 10.1021/jacs.7b02736

Zhao, S., Wang, Y., Dong, J., He, C. T., Yin, H., An, P., et al. (2016). Ultrathin metal–organic framework nanosheets for electrocatalytic oxygen evolution. *Nat. Energy.* 1:16184. doi: 10.1038/nenergy.2016.184

Zhou, H., Yu, F., Zhu, Q., Sun, J., Qin, F., Yu, L., et al. (2018). Water splitting by electrolysis at high current densities under 1.6 volts. *Energy Environ. Sci.* 11, 2858–2864. doi: 10.1039/C8EE00927A

Zhuang, L., Ge, L., Yang, Y., Li, M., Jia, Y., Yao, X., et al. (2017). Ultrathin iron-cobalt oxide nanosheets with abundant oxygen vacancies for the oxygen evolution reaction. *Adv. Mater.* 29:06793. doi: 10.1002/adma.201606793

Conflict of Interest: The authors declare that the research was conducted in the absence of any commercial or financial relationships that could be construed as a potential conflict of interest.